Available online at www.sciencedirect.com

ScienceDirect

Procedia Structural Integrity 28 (2020) 1481–1502

Structural Integrity Procedia

www.elsevier.com/locate/procedia

1st Virtual European Conference on Fracture

Austempered ductile iron-to-steel dissimilar arc-welded joints: fatigue strength assessment according to local approaches

Giovanni Meneghetti[1]*, Alberto Campagnolo[1], Elena Pullin[1], Stefano Masaggia[2]

[1]*Department of Industrial Engineering, University of Padova, Via Venezia, 1 – 35131 Padova (Italy)*
[2]*Zanardi Fonderie Spa, Via Nazionale 3, 37046 Minerbe (Verona - Italy)*

Abstract

The design of mechanical components increasingly requires the adoption of different materials in the same structure with the aim of improving its performance. One of the available solutions is to adopt dissimilar arc-welded joints, which typically must withstand high fatigue loadings during in-service life. In a recent paper, the fatigue strength of EN-JS-1050 austempered ductile iron-to-S355J2 steel dissimilar arc-welded joints was experimentally investigated by testing some typical welded details in the as-welded conditions, under either axial or four-point bending loadings. In the present work, previous experimental campaign has been extended by fatigue testing other ADI-to-steel joint details. The fracture surfaces of all tested joints have been analysed to identify the fatigue crack initiation locations. Then, experimental fatigue results have been re-analysed to determine the fatigue strength category of each welded detail, which have been compared with those provided by International Standards for corresponding homogeneous steel joints. Afterwards, the local approach based on the Peak Stress Method (PSM) combined with the averaged Strain Energy Density (SED) fatigue criterion, has been used for the first time for fatigue strength assessment of ADI-to-steel dissimilar arc-welded joints. First, the structural volume size R_0 has been calibrated for joints exhibiting fatigue crack initiation and propagation at the ADI side; then, a PSM-based fatigue design curve has been determined by fitting the available experimental results.

Keywords: dissimilar welded joints; austempered ductile iron; structural steel; fatigue behaviour; Peak Stress Method

* Corresponding author. Tel.: 0039 049 827675; fax: 0039 049 8276785.
E-mail address: giovanni.meneghetti@unipd.it

10.1016/j.prostr.2020.10.122

1. Introduction

In several industrial sectors, the design of mechanical components increasingly requires the combination of different materials into a multi-material structure. The properties of each material are jointly employed to design high-performance components and to integrate an higher number of functions. However, joining together materials which have different chemical, mechanical, thermal, or electrical properties intrinsically yields great challenges. The possible incompatibility of physical or mechanical properties, such as thermal expansion, ductility, fatigue strength, elastic modulus etc, could negatively influence the joining process itself, but also the integrity of the structure under service conditions. Martinsen et al. (Martinsen et al., 2015) recently reviewed advantages and challenges of joining dissimilar materials.

A solution to obtain a multi-material structure could be to weld components made of different materials. Among the available welding techniques, the most used ones for this purpose are:

- friction-welding (Figner et al., 2009; Infante et al., 2016; Mohammadzadeh Polami et al., 2015; Okamura and Aota, 2004; Taban et al., 2010; Uzun et al., 2005);
- arc-welding (Al Zamzami et al., 2019; Kumar et al., 2017; Roberts et al., 1985; Zhang et al., 2018).

Dealing with arc-welding, joining Austempered Ductile Iron (ADI) to dissimilar structural steel allows to improve the mechanical response of the multi-material structure, due to the combination of weight reduction and net-to-shape geometry. Indeed, ADI has optimum static, impact, fatigue performances and moderate wear resistance. Moreover, its excellent castability allows to design complex geometries combined with great lightweight characteristics. This leads to the optimization of mass distribution based on both actual stiffness and required load levels, thus reducing the use of steel where needed or mandatory.

Dissimilar joints need to withstand high fatigue loadings during in-service life. International Standards and Recommendations (*Eurocode 3: Design of steel structures – part 1–9: Fatigue*, 2005, *Eurocode 9: Design of aluminium structures - Part 1-3: Structures susceptible to fatigue*, 2011; Hobbacher, 2016) provide several approaches for fatigue design of welded joints: the nominal stress, the hot-spot stress, the notch stress and the Linear Elastic Fracture Mechanics (LEFM) approaches. The nominal stress approach is based on stress calculations according to solid mechanics and it is the most widely adopted. Accordingly, the fatigue strength assessment of a welded joint is carried out by comparison of the nominal stress with the relevant design category, which is a function of the joint geometry and loading condition. However, International Standards and Recommendations (*Eurocode 3: Design of steel structures – part 1–9: Fatigue*, 2005, *Eurocode 9: Design of aluminium structures - Part 1-3: Structures susceptible to fatigue*, 2011; Hobbacher, 2016) report fatigue strength categories for applying the nominal stress approach only to homogeneous welded joints made of either structural steels or aluminum alloys and not for dissimilar joints. Due to the lack of information in the relevant literature and in International Standards and Recommendations, a preliminary investigation of the fatigue behaviour of austempered ductile iron (EN-JS-1050)-to-steel (S355J2) arc-welded joints has been performed by testing some typical joint details in recent papers of the present authors (Meneghetti et al., 2019a, 2019b). In the present work, previous experimental campaign has been extended by fatigue testing other typical joint details and by deriving the fatigue strength categories of all tested details in terms of nominal stress range.

However, it is widely recognized that local approaches (Radaj et al., 2006) allow to obtain the best level of accuracy for the fatigue assessment of welded components. Among them, the approach based on Notch Stress Intensity Factors (NSIFs) (Atzori and Meneghetti, 2001; Lazzarin and Livieri, 2001; Lazzarin and Tovo, 1998) and on the averaged strain energy density (SED) (Livieri and Lazzarin, 2005), the approaches based on critical plane concept (Carpinteri et al., 2009; Sonsino, 1995; Susmel, 2009) and the Theory of Critical Distances (TCD) (Susmel, 2008; Taylor et al., 2002) are the most widely employed. Accordingly, in the present paper the local approach based on the combination of the Peak Stress Method (PSM) (Meneghetti and Lazzarin, 2007) with the averaged Strain Energy Density (SED) fatigue criterion, has been calibrated for the first time to the fatigue strength assessment of austempered ductile iron-to-steel dissimilar arc-welded joints.

Finally, the aims of the present paper are:

- to extend previous experimental campaign by fatigue testing other ADI-to-steel joint details and by analyzing the fracture surfaces of the joints to identify the fatigue crack initiation locations;
- to derive the fatigue strength categories of all tested welded details and to compare them with the categories provided by standards and recommendations for corresponding homogeneous welded steel joints;
- to calibrate the structural volume size R_0 for ADI-to-steel arc-welded joints;

- to derive a PSM-based fatigue design curve valid for ADI-to-steel arc-welded joints by fitting the available experimental results.

2. Testing program

S355J2 EN10025-2 hot rolled construction steel (S355J2) is widely employed in structural applications, while ISO 17804 JS/1050-6 Austempered Ductile Iron (ADI 1050) is typically adopted in earth movement undercarriage components, suspension parts, axles, power transmission components, etc.

ADI 1050 is produced by heat-treating a low alloyed Pearlitic-Ferritic Ductile Iron, cast after a special preconditioning of the metal bath. The cast material is made of iron where carbon is mainly present in the form of spheroidal graphite particles. The isothermal heat treatment of spheroidal graphite cast iron, known as "Austempering", basically consists in heating the castings at 900°C and, after that, cooling it in salt bath having constant temperature of 350 °C, at a cooling rate able to promote the formation of "Ausferrite". This process generates a microstructure which consists mainly of retained austenite and acicular ferrite. The matrix is called "Ausferritic" and provides to the new material mechanical properties which are comparable to a 42CrMo4Q&T steel.

The fatigue tested joint geometries are reported in Fig. 1 along with details about the loading conditions, the testing conditions being described in more detail in next Section 5 and Table 3. It is worth noting that series A, B1, B2 and C were fatigue tested in previous works (Meneghetti et al., 2019a, 2019b), while all other series have been fatigue tested in the present investigation. For completeness, the experimental fatigue results generated from all test series will be analysed in the following.

3. Preparation of welded specimens

All specimens were manufactured from plates having dimensions 300x150x12 mm. Ductile iron plates were poured by Zanardi Fonderie S.p.A. in horizontal greensand moulds printed using a proper experimental pattern plate; they were sand cleaned after shakeout, austempered to material grade ADI 1050 and milled to the final thickness of 10 mm.

Steel plates, having same initial dimensions, were obtained from commercial hot rolled plates and then reduced to 10 mm thickness by milling.

All plates were grinded, brushed and properly clamped by means of tack welded fixture bracket in order to minimize welding distortions. Final specimen's dimensions were obtained by cutting after welding. All welding operations were done by 'Istituto Italiano della Saldatura' (IIS).

ADI 1050 showed ultimate strength R_m=1100 MPa, yield strength R_{p02}=920 MPa, Brinell hardness HBW=350÷380 and elongation at fracture A_5=8%; all mechanical properties were obtained from specimens cut from the plates. S355J2 mechanical properties according to EN10025-2 are ultimate strength $R_{m\ min}$=470 MPa, yield strength $R_{p02\ min}$=355 MPa, HBW=160÷180 and elongation at fracture $A_{5\ min}$=22%.

3.1 Manufacturing of specimens

Welding parameters were tuned in (Meneghetti et al., 2019a, 2019b) by taking into account the specimen's thickness of 10 mm, weld bead size, misalignments, runs number and all different types of joint details investigated. The main issue was to prevent martensite formation and cracks nucleation within HAZ of ADI 1050: the proper set of welding parameters was identified in such a way that the resulting hardness was as close as possible to the base ADI material. However, the formation of ledeburite layer close to the weld metal cannot be avoided as in this area ductile iron always undergoes metastable solidification after re-melting. The complete set of welding parameters is reported in Table 1. In particular, pulsed arc fully mechanized GMAW-welding process was adopted.

Table 2 summarizes the specimens' geometry and preparation. Macrographic/micrographic tests as well as VT, PT and HBW test were carried out on all specimens as reported in (Meneghetti et al., 2019a, 2019b). Quality level for imperfections was according to ISO 5817-B.

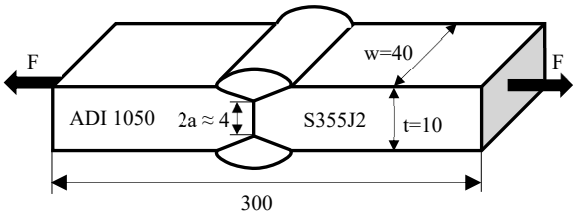

A: partial-penetration butt-welded joints under axial loading

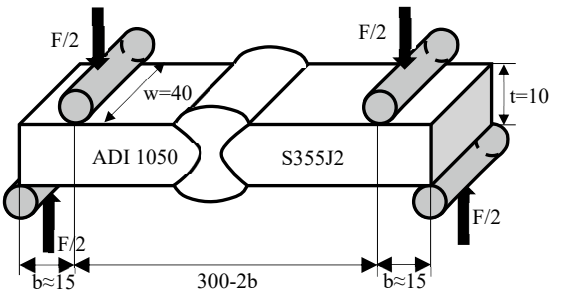

B1: full-penetration butt-welded joints under 4PB loading

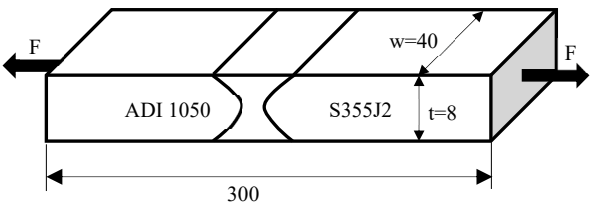

B2: full-penetration ground butt-joints under axial loading

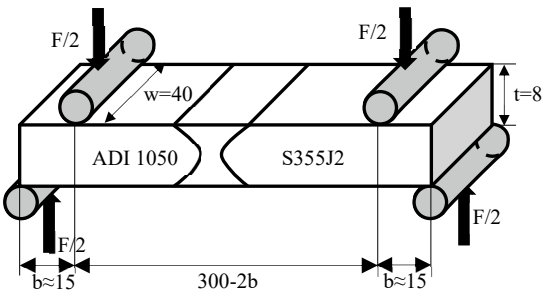

B2: full-penetration ground butt-joints under 4PB loading

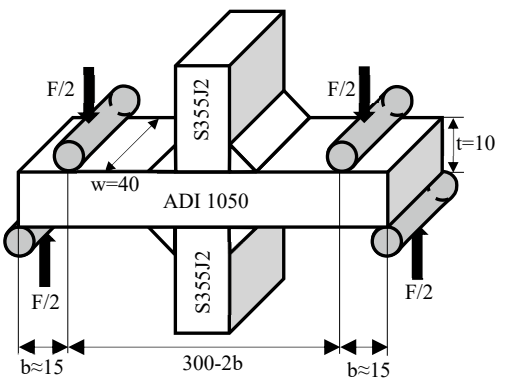

C: cruciform non-load-carrying fillet-welded joints under 4PB loading

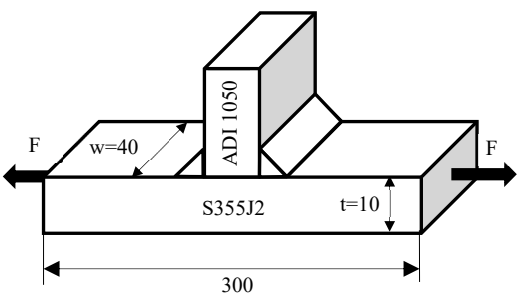

D: T non-load-carrying fillet-welded joints under axial loading

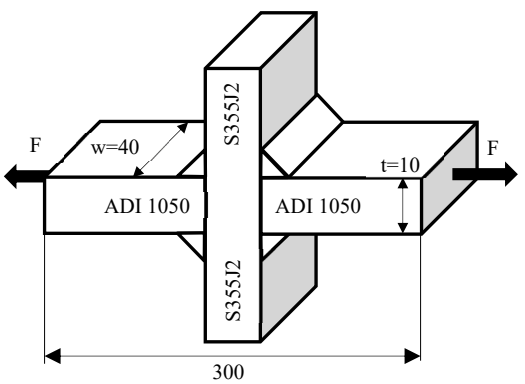

E: cruciform load-carrying fillet-welded joints under axial loading

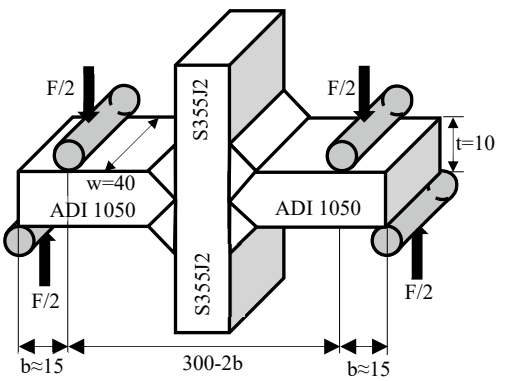

F: cruciform full-penetration k-butt welded joints under 4PB loading

Figure 1: Geometries and loading conditions of dissimilar welded joints tested under fatigue loading.

Table 1: GMAW welding parameters adopted for production of specimens

Mode of metal transfer	Welding position	Torche angle direction	Filler material	Current& Polarity [A]	Voltage [V]	Travel speed [mm/min]	Heat input [kJ/mm]
P	UNI EN ISO 6947 PA	15° forehand	S C NiFe-2 EN ISO 1071 ø 1.2 mm	CCPI 120÷130	24÷25	220÷340	0.41÷0.71

Preheat temperature	EN 13916-TC 200°C
Interpass temperature	EN 13916-TC 250°C
Shielding	ISO 14175 M21 (Ar-CO_2 80-20), flow rate 16÷18 lt/min

Table 2: Specimens' geometry and preparation

Type of joint		Macrograph & HBW position
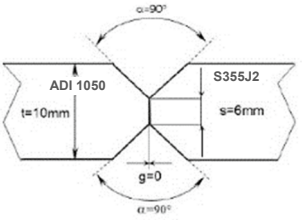 A: partial-penetration butt joint	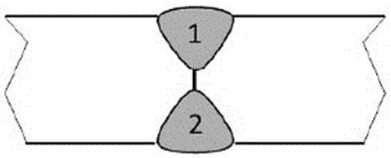	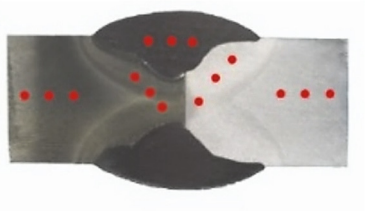
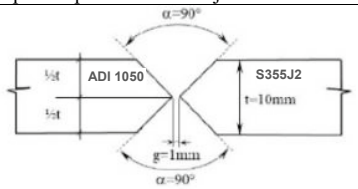 B1: full penetration butt joints B2: full penetration ground butt joints	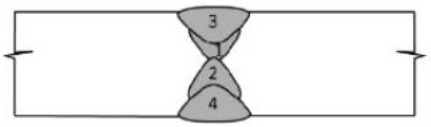	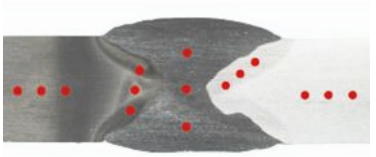
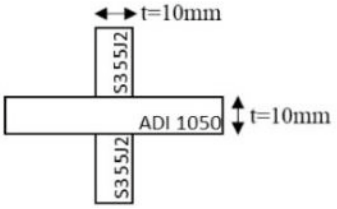 C: cruciform non-load-carrying fillet-welded joints	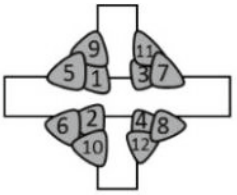	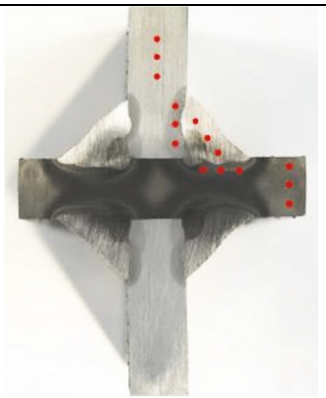

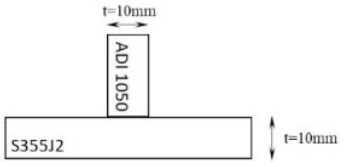

D: T non-load-carrying fillet-welded joints

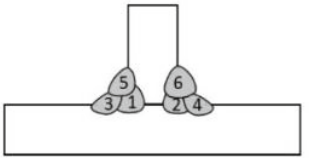

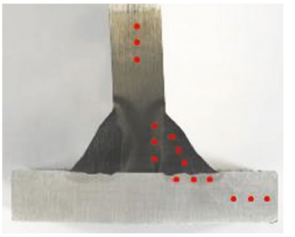

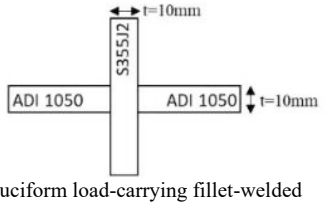

E: cruciform load-carrying fillet-welded joints

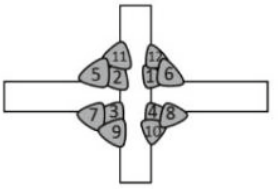

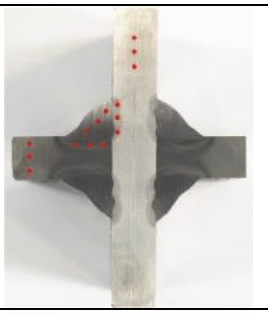

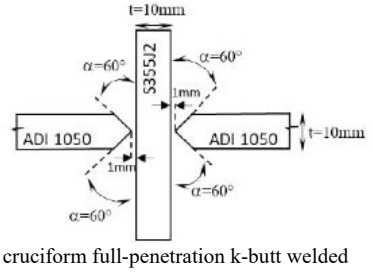

F: cruciform full-penetration k-butt welded joints

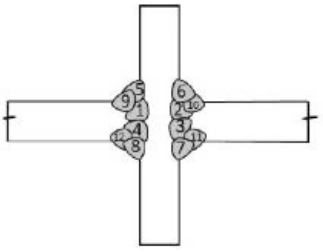

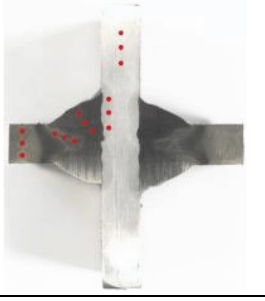

4. Specimen characterisation

Micro-hardness and residual stress profiles, along with misalignments, were measured for all ADI-to-steel joint details with the aim of evaluating the conditions of post-weld materials. However, for the sake of brevity, only the hardness measurements are reported in the present paper, more details being available in (Meneghetti et al., 2019a, 2019b), to which the reader is referred.

Vickers hardness HV1 profiles have been measured to recognize microstructural alterations. For sake of brevity, only the results relevant to joint detail C (cruciform nlc fillet-welded joint) are reported in Fig. 2, the results for the other joint geometries being similar (Meneghetti et al., 2019a, 2019b). The results confirm that heat affected zone of ADI 1050 primarily consists of graphite nodules in pearlitic matrix and ledeburite layer close to weld metal; HAZ of S355J2 consists of ferritic-pearlitic matrix.

5. Fatigue tests

5.1 Testing parameters

Experimental fatigue tests have been carried out on joint details shown in Figure 1, adopting the testing conditions reported in Table 3. Based on the measured misalignments (Meneghetti et al., 2019a, 2019b), the loading conditions have been applied to each test series as follows (see Fig. 1):

- series A and E have been fatigue tested under axial loading to assess weld root as well as weld toe failure. To do so, the clamping surfaces have been milled (Meneghetti et al., 2019a, 2019b) to minimize the misalignments and reduce secondary bending effects;

- series B1, C and F, have been tested under four-point bending loading, in order to avoid secondary bending effects;
- series B2, have been tested under both axial loading and four-point bending loading, as misalignments had been previously removed by milling the specimen surfaces to remove the weld caps;
- series D have been tested under axial loading, since misalignments were reduced.

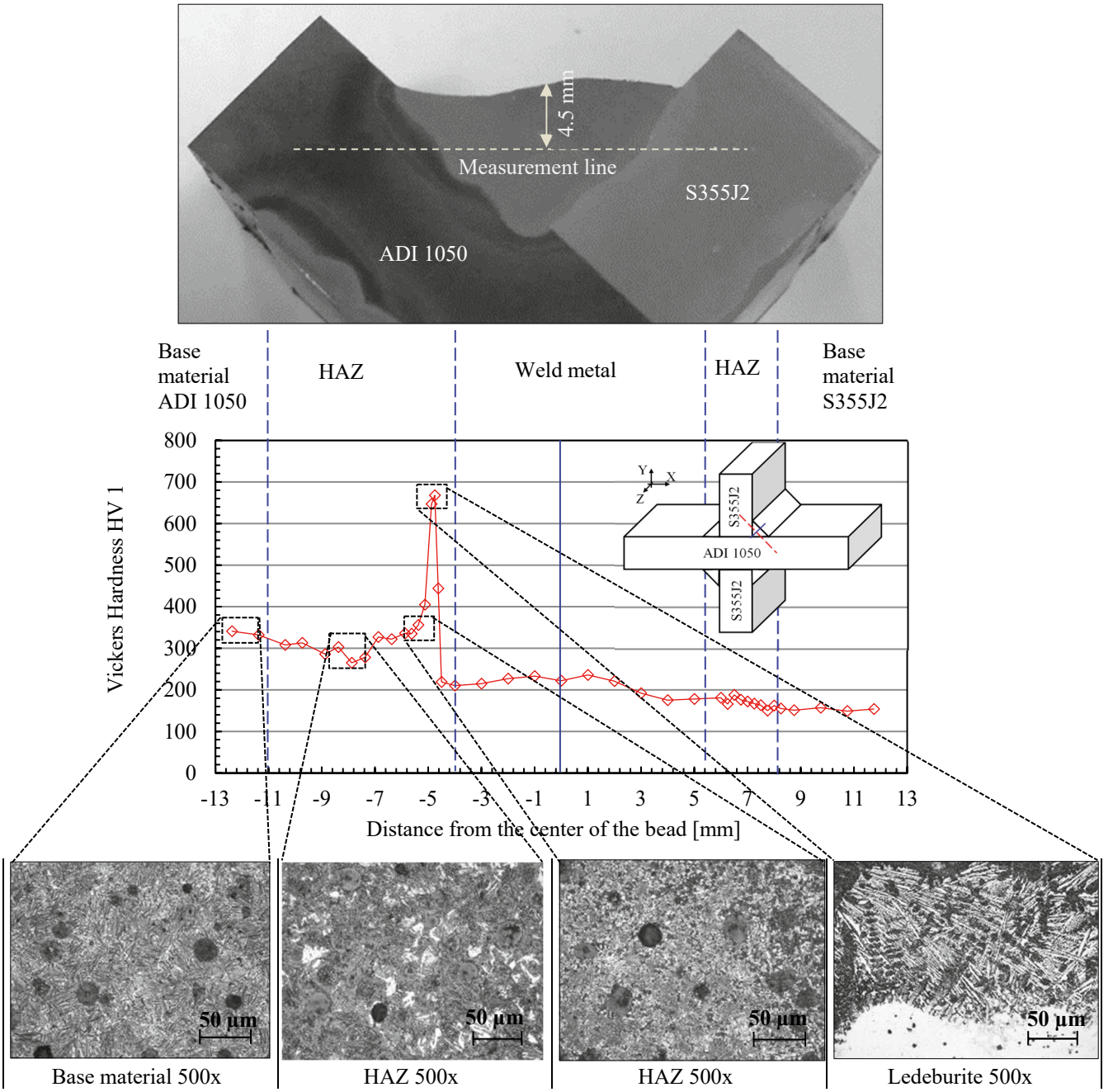

Figure 2: HV1 measurement on cross-section of a joint type C (cruciform nlc fillet-welded joint)

The experimental fatigue tests have been carried out in standard laboratory environment using a MFL axial servo-hydraulic machine, with a load capacity of 250 kN and being equipped with a MTS TestStar IIm digital controller. The experimental fatigue tests have been carried out under closed-loop load control by imposing a constant amplitude sinusoidal load cycle with a nominal load ratio R as reported in Table 3. The load frequency has been set in the range 10÷30 Hz as a function of the applied load level. Fatigue failure of each joint has been defined as the number of loading cycles N_f at complete separation, while run-out has been fixed at $2 \cdot 10^6$ cycles, if no failure was detected.

Table 3: Testing conditions of the welded joints and summary of test results.

Specimen code	Joint detail	Testing condition*	tested specimens	Load#	Nominal load ratio R	failure criterion	$\Delta\sigma_A^{\circ}$ [MPa]	k	T_σ
A	Partial-penetration butt joints	AW	12 4	Ax	0.05 0.5	complete separation	73	4.71	1.98
B1	Full-penetration butt joints		13	4PB	0.05		159	8.84	1.99
B2	Full-penetration ground butt-joints		5 6	Ax 4PB	0.05 0.05		228 251	27.9 8	1.6 1.72
C	Cruciform nlc fillet-welded joints		17 10	4PB	0.05 0.5		169	11	2.68
D	T non-load-carrying fillet-welded joints		12 2	Ax	0.05 0.5		110	5	2.47
E	Cruciform load-carrying fillet-welded joints		8 4	Ax	0.05 0.5		96	11.24	2.53
F	Cruciform full-penetration k-butt welded joints		8 2	4PB	0.05 0.5		77	4.52	3.36

° endurable stress range referred to a survival probability of 97.7% and N_A=2 million loading cycles
* AW = as welded
# Ax=axial load, 4PB=four-point bending load

5.2 Damage analysis

Some examples of the fracture surfaces obtained after fatigue tests are reported in Figs. 3-9 for each test series.

Concerning partial-penetration butt-joints, multiple fatigue crack initiation locations were observed, as shown in the examples of Fig. 3. Fatigue cracks mainly initiated at the root side, then propagated through the weld throat inside the steel region. Additional propagating fatigue cracks were observed at the weld toe at the ADI side as well as at the interface between the ADI plate and the weld bead.

Full-penetration butt-joints exhibited fatigue crack initiation always at the weld toe at the ADI side as shown in Fig. 4, then fatigue crack propagated along the thickness of the joint.

Dealing with full-penetration ground butt-joints, the fatigue cracks always initiated at the interface between the ADI plate and the weld bead as shown in Fig. 5, then propagated along the thickness of the joint.

In the case of cruciform nlc (Fig. 6) and lc (Fig. 8) fillet-welded joints and full-penetration k-butt welded joints (Fig. 9), the fatigue cracks always initiated at the weld toe at the ADI side, then propagated along the thickness of the joint.

Finally, T non-load-carrying fillet-welded joints exhibited fatigue crack initiation always at the weld toe at the steel side as shown in Fig. 7, then propagated along the thickness of the joint.

The fracture surfaces of the joints exhibiting crack initiation at ADI side have furtherly been analysed by optical microscopy and the results have been reported in Figs. 4-6, 8-9. It can be observed that in all considered cases, fatigue crack initiation always occurred at weld toe side in the ledeburite region, where the hardness is about 700HV as compared to 350-400HV of the ADI base material (see Fig. 2). Then fatigue crack propagates within the ausferrite decomposed region.

5.3 Fatigue results

The fatigue results are reported in Fig. 10 in terms of number of cycles versus the applied nominal stress range Δσ (defined as maximum value minus minimum value). It should be noted that in the case of partial-penetration butt-joints under axial loading (Fig. 10a), the nominal stress range Δσ has been calculated in the weld throat area according to the following expression (see dimensions in Fig. 1):

$$\Delta\sigma = \frac{\Delta F}{A_{throat}} = \frac{\Delta F}{W(t-2a)} \quad (1)$$

In all other cases (Fig. 10b-h), the nominal stress range has been calculated in the gross section.

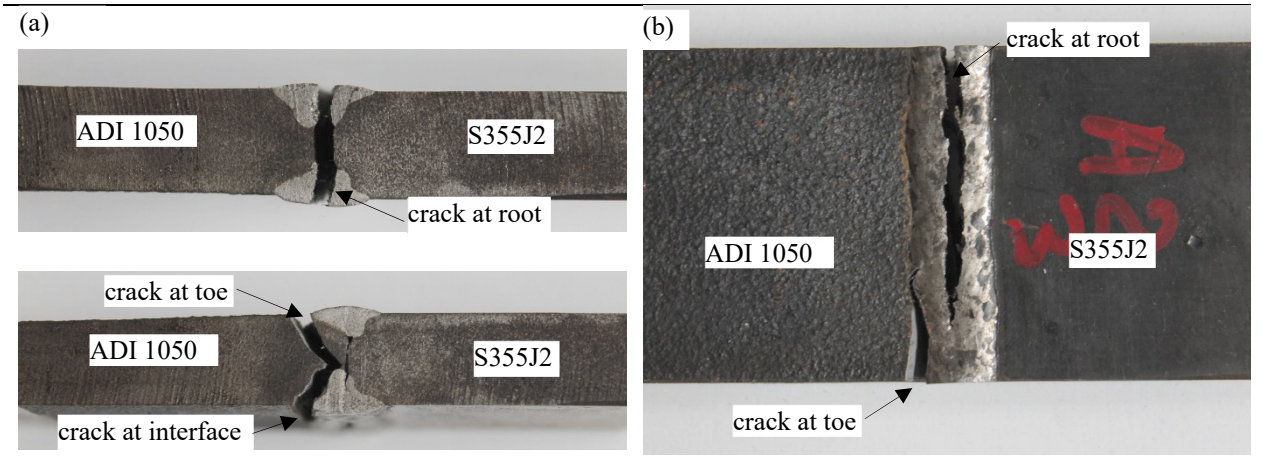

Specimen code: A_2_3, AW, Axial loading, R= 0.05, Δσ = 105.6 MPa, N_f = 1926134 cycles

Figure 3: Fracture surfaces of partial-penetration butt-joints tested under axial fatigue loading.

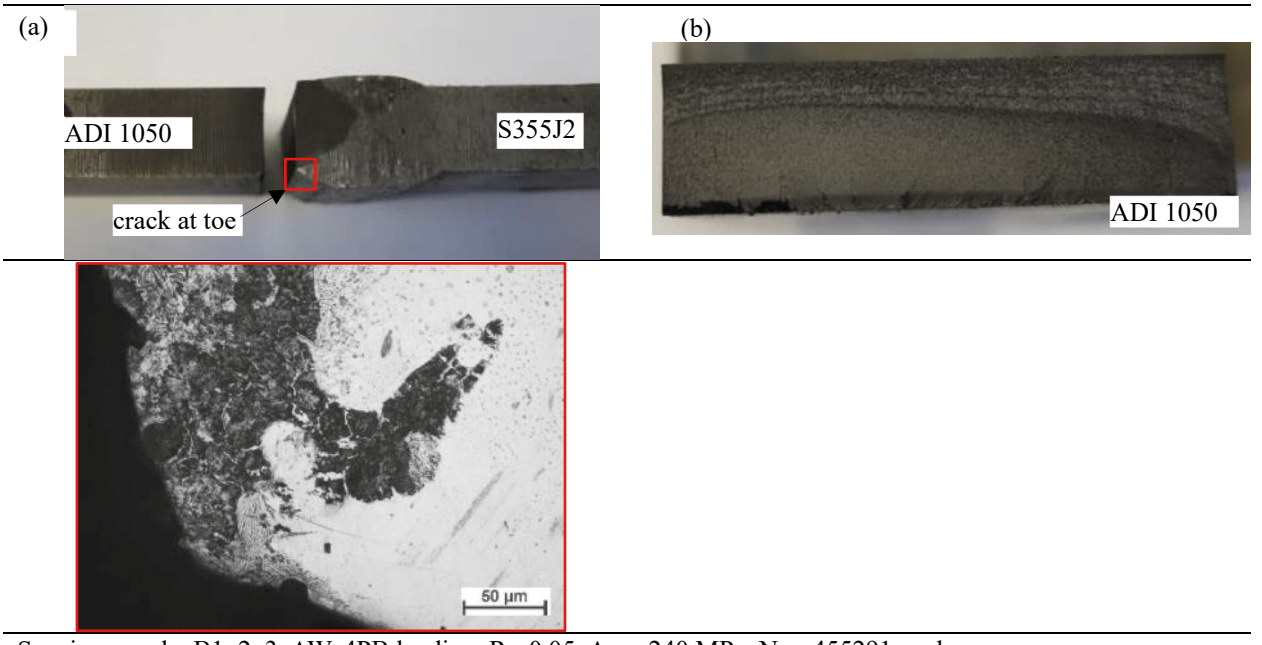

Specimen code: B1_2_3, AW, 4PB loading, R= 0.05, Δσ = 240 MPa, N_f = 455291 cycles

Figure 4: Fracture surfaces of full-penetration butt-joints tested under four-point-bending fatigue loading.

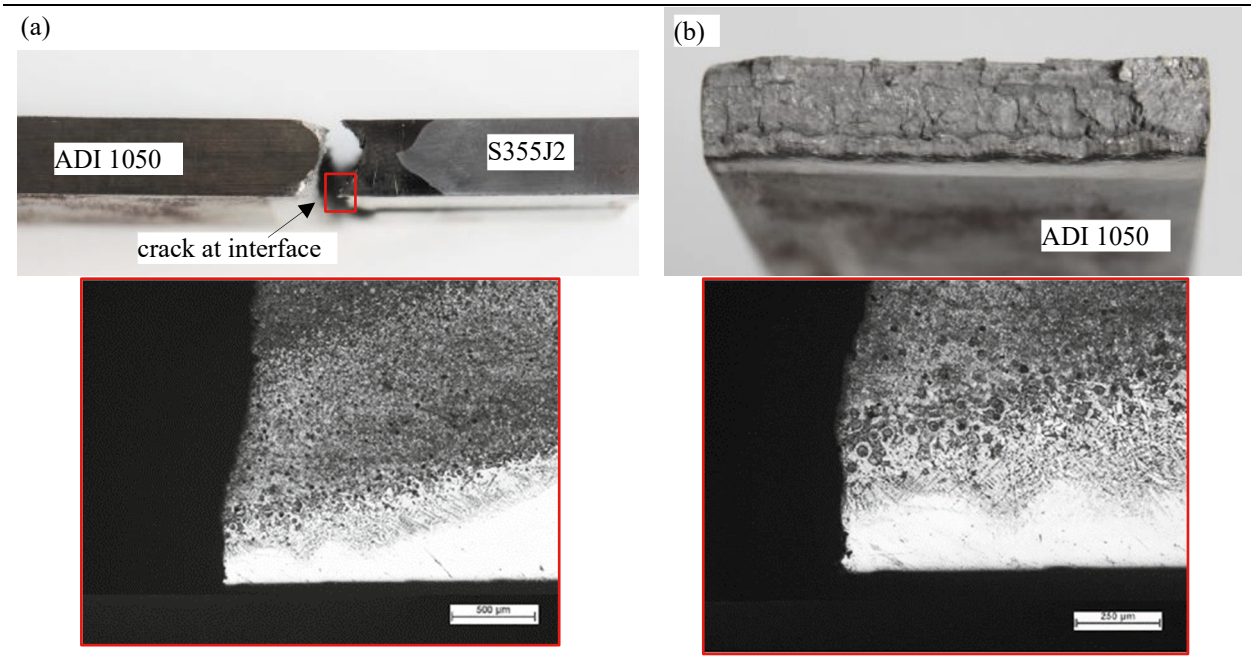

Specimen code: B2_4_2, AW, Axial loading, R= 0.05, $\Delta\sigma$ = 320 MPa, N_f = 109630 cycles

Figure 5: Fracture surfaces of full-penetration ground butt-joints tested under axial fatigue loading.

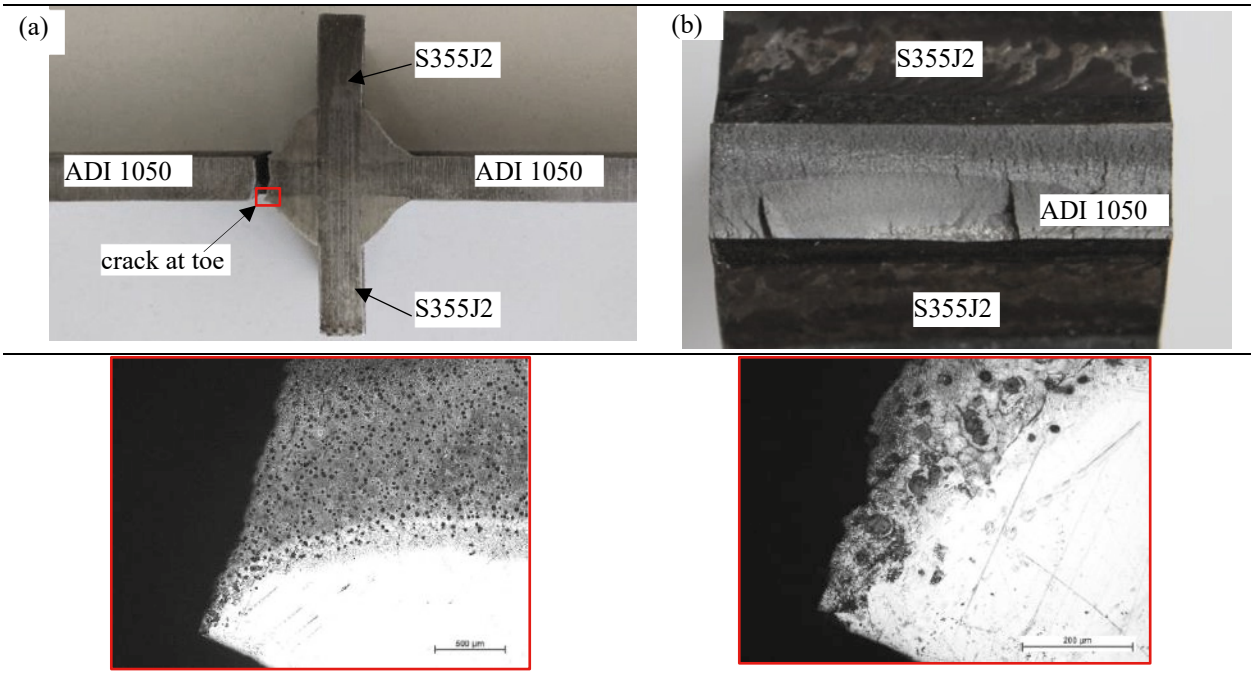

Specimen code: C_11_1, AW, 4PB loading, R= 0.05, $\Delta\sigma$ = 322 MPa, N_f = 782127 cycles

Figure 6: Fracture surfaces of cruciform nlc fillet-welded joints tested under four-point-bending fatigue loading.

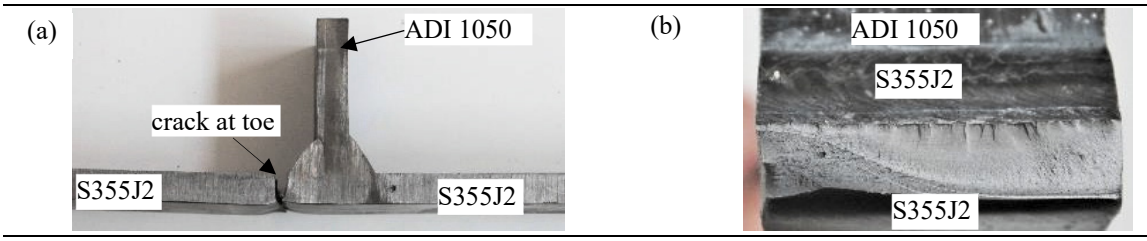

Specimen code: D_1_1, AW, Axial loading, R= 0.05, $\Delta\sigma$ = 235 MPa, N_f = 353034 cycles

Figure 7: Fracture surfaces of T non-load-carrying fillet-welded joints tested under axial fatigue loading.

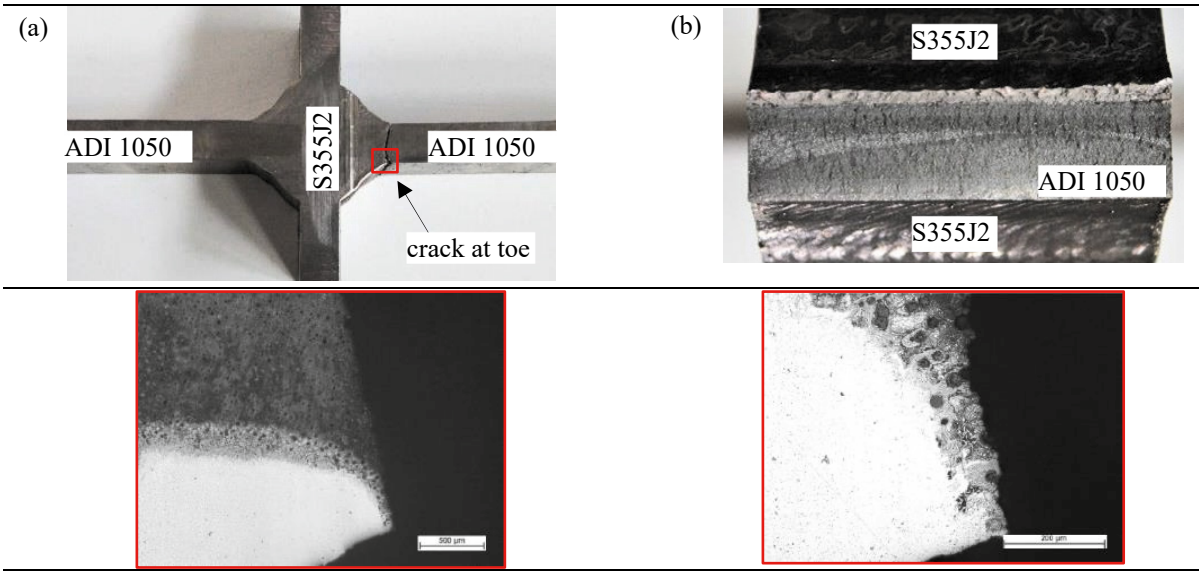

Specimen code: E_2_1, AW, Axial loading, R= 0.05, $\Delta\sigma$ = 192 MPa, N_f = 256157 cycles

Figure 8: Fracture surfaces of cruciform load-carrying fillet-welded joints tested under axial fatigue loading.

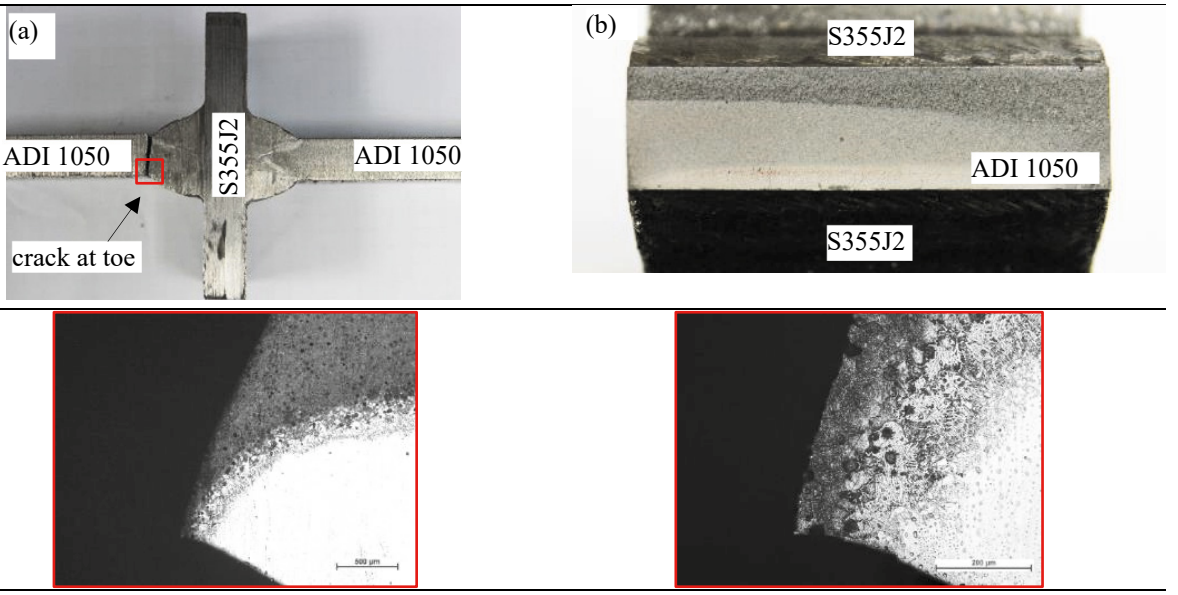

Specimen code: F_4_3, AW, 4PB loading, R= 0.05, $\Delta\sigma$ = 192 MPa, N_f = 1222986 cycles

Figure 9: Fracture surfaces of cruciform full-penetration k-butt welded joints tested under four-point-bending fatigue loading.

The scatter bands reported in Figs. 10 are referred to survival probabilities of 2.3 and 97.7% and to a 95% confidence level. The endurable stress ranges at 2 million loading cycles for a survival probability 97.7%, the inverse slope k, and the scatter index T_σ are summarised in Table 3. Figure 10 shows that all tested details exhibit an endurable stress range, which is referred to a survival probability of 97.7% and 2 million loading cycles, higher than the FAT values suggested by Eurocode 3 and IIW Recommendations (*Eurocode 3: Design of steel structures – part 1–9: Fatigue*, 2005; Hobbacher, 2016) for corresponding homogeneous joints made of structural steels, especially at the high cycle fatigue regime. On the other hand, the fatigue strength of ADI-to-steel joints is significantly lower than that of homogeneous joints made of structural steels at medium cycle fatigue regime.

Finally, the experimental results generated from ADI-to-steel joints exhibiting fatigue failure at weld toe at ADI side have been summarised in Fig. 11, which includes also a 2.3-97.7% scatter-band calibrated on all considered experimental results. The resulting fatigue design curve is characterised by a fatigue class of $\Delta\sigma_{A,97.7\%} = 94$ MPa, an inverse slope k = 10 and a scatter index $T_\sigma = 5$. It is worth noting that a synthesis of experimental fatigue results generated by different joint geometries and expressed in terms of nominal stress range provides a very high scatter index, which could translate in a significant oversizing of the designed welded structure.

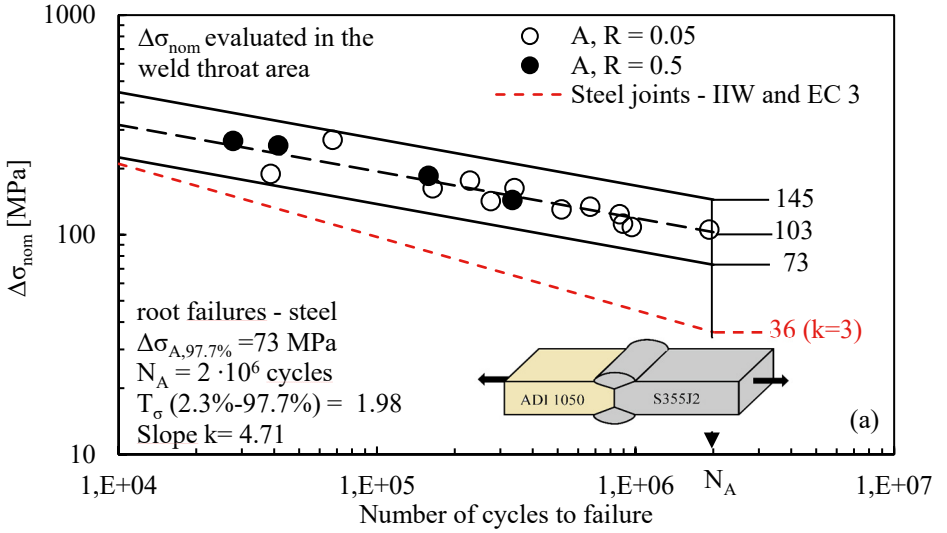

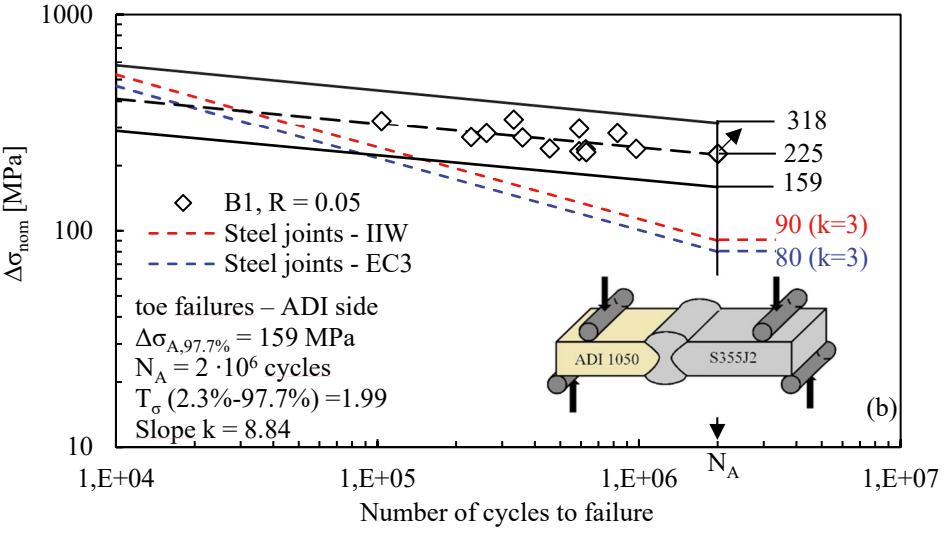

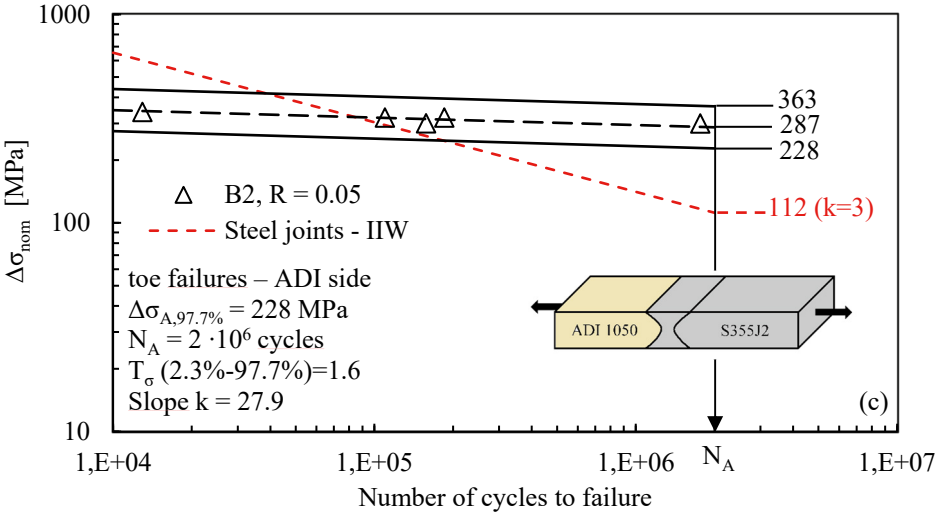
1000
100
10
$\Delta\sigma_{nom}$ [MPa]
363
287
228
112 (k=3)
B2, R = 0.05
Steel joints - IIW
toe failures – ADI side
$\Delta\sigma_{A,97.7\%}$ = 228 MPa
$N_A = 2 \cdot 10^6$ cycles
T_σ (2.3%-97.7%)=1.6
Slope k = 27.9
ADI 1050
S355J2
(c)
1,E+04
1,E+05
1,E+06
N_A
1,E+07
Number of cycles to failure

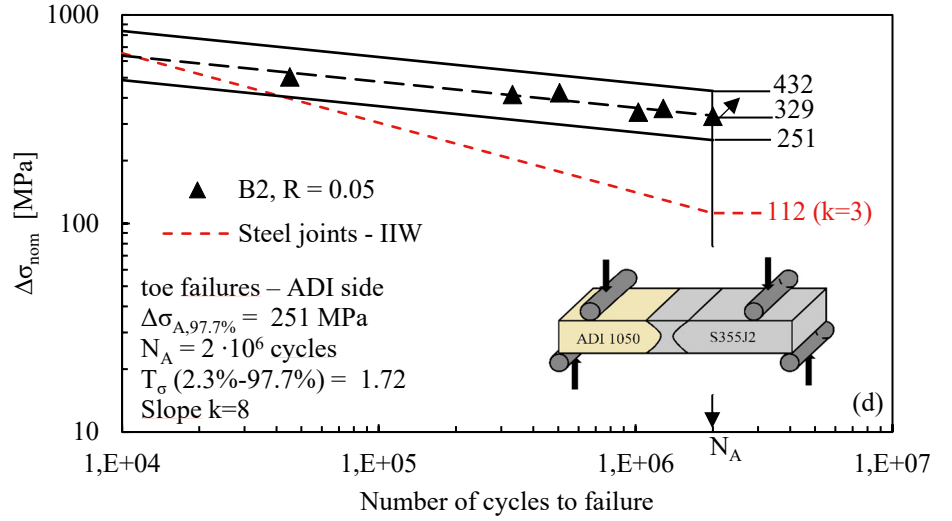
1000
100
10
$\Delta\sigma_{nom}$ [MPa]
432
329
251
112 (k=3)
B2, R = 0.05
Steel joints - IIW
toe failures – ADI side
$\Delta\sigma_{A,97.7\%}$ = 251 MPa
$N_A = 2 \cdot 10^6$ cycles
T_σ (2.3%-97.7%) = 1.72
Slope k=8
ADI 1050
S355J2
(d)
1,E+04
1,E+05
1,E+06
N_A
1,E+07
Number of cycles to failure

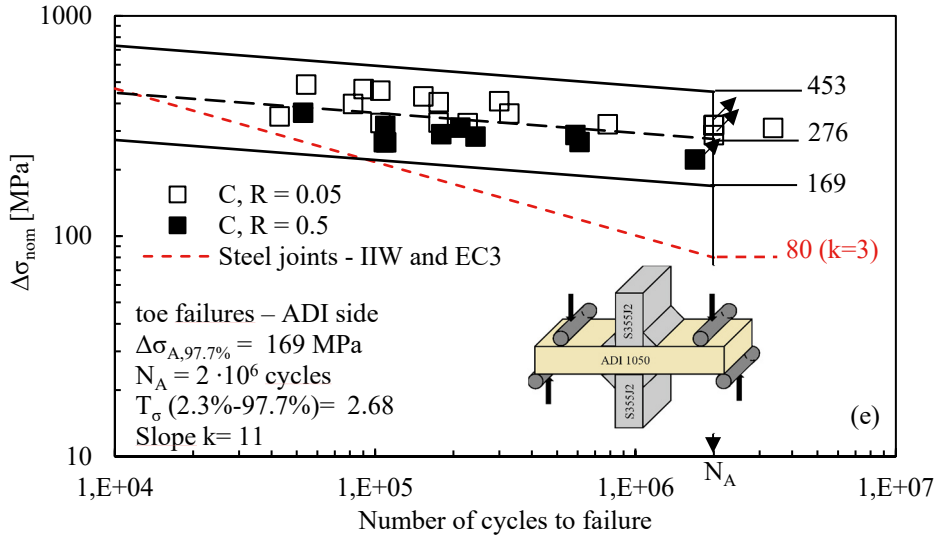
1000
100
10
$\Delta\sigma_{nom}$ [MPa]
453
276
169
80 (k=3)
C, R = 0.05
C, R = 0.5
Steel joints - IIW and EC3
toe failures – ADI side
$\Delta\sigma_{A,97.7\%}$ = 169 MPa
$N_A = 2 \cdot 10^6$ cycles
T_σ (2.3%-97.7%)= 2.68
Slope k= 11
S355J2
ADI 1050
S355J2
(e)
1,E+04
1,E+05
1,E+06
N_A
1,E+07
Number of cycles to failure

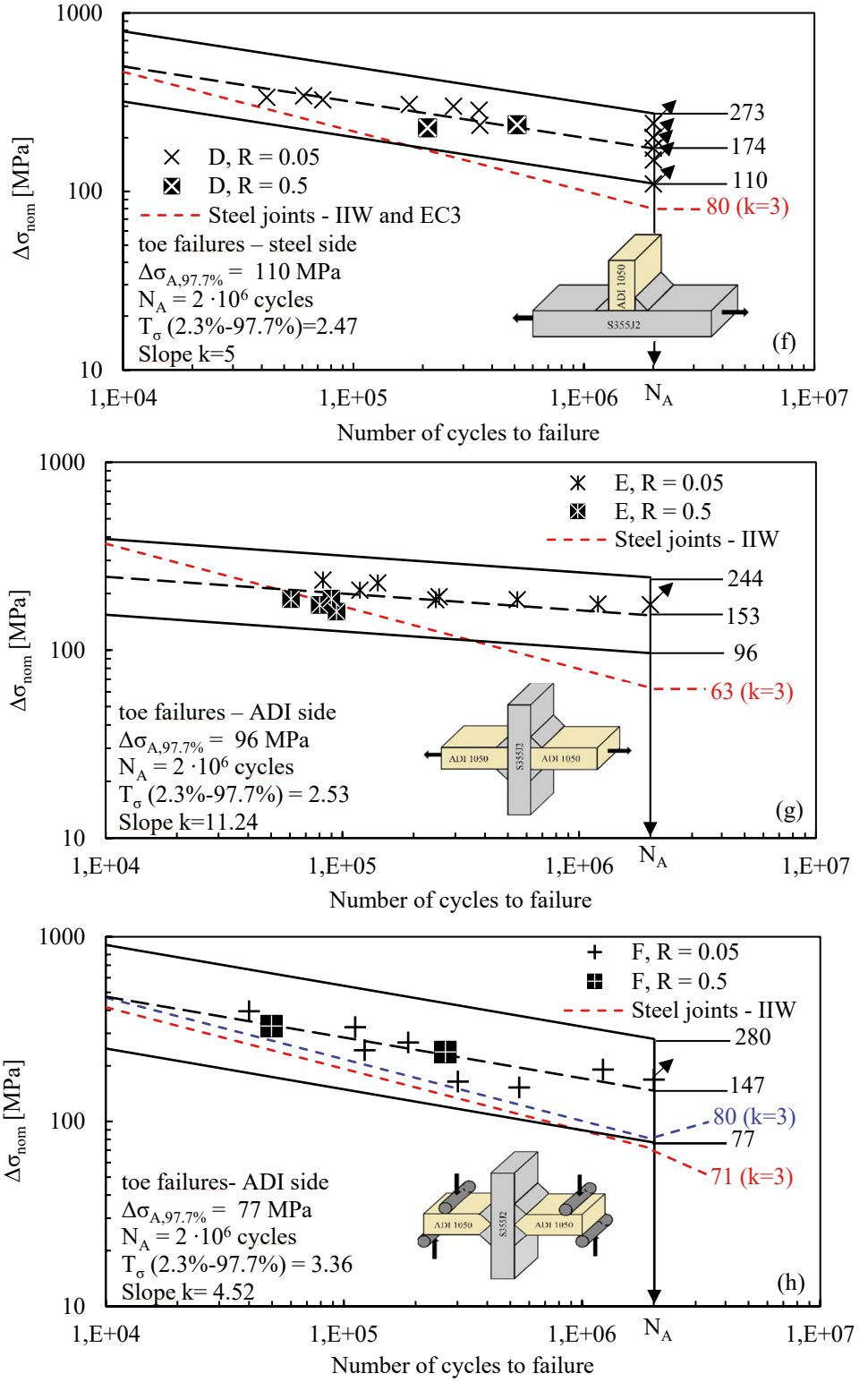

Figure 10: Experimental results of fatigue tests performed on (a) partial-penetration butt joints, (b) full-penetration butt joints, (c) and (d) full-penetration ground butt-joints, (e) cruciform nlc fillet-welded joints, (f) T non-load-carrying fillet-welded joints, (g) cruciform load- carrying fillet-welded joints, (h) cruciform full-penetration k-butt welded joints.

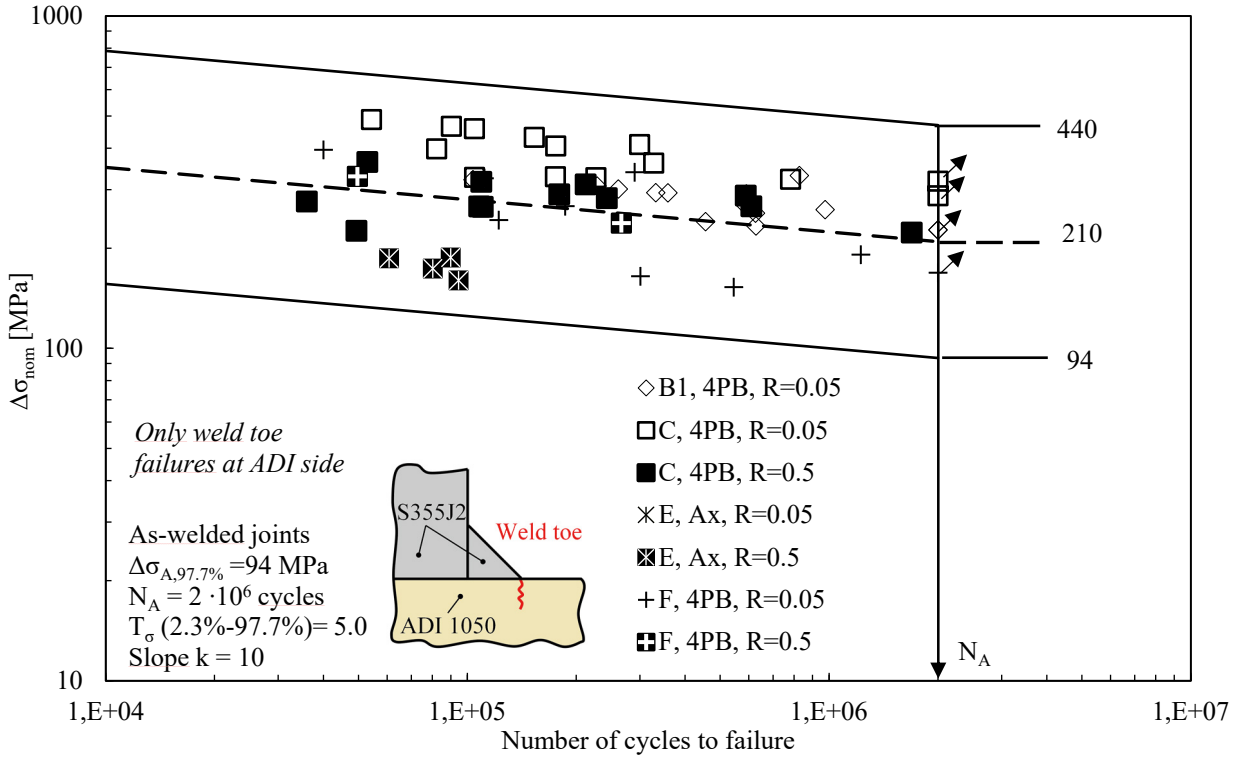

Figure 11: Synthesis of experimental results relevant only to fatigue crack initiation at the weld toe at ADI side (Figs. 10b,e,g,h) in terms of number of cycles to failure as a function of the range of the nominal stress.

6. Fatigue strength assessment according to local approaches

6.1 Theoretical background

According to the local fatigue approach based on the Notch Stress Intensity Factors (NSIFs) (Lazzarin and Tovo, 1998; Radaj et al., 2006), a worst-case condition corresponding to a sharp V-notch having null tip radius (ρ = 0) is assumed both at the weld toe and at the weld root of a joint detail, the toe and root sides being modelled with opening angles of 135° and 0°, respectively, as highlighted in Fig. 12a. Given these idealisations and assuming a linear-elastic behaviour of the material, an external load applied to a welded structure generates singular stress fields in the local material regions closed to both toe and root sides. The mode I NSIF, which can be defined according to (Gross and Mendelson, 1972) by means of Eq. (1), allow to quantify the intensity of these stress distributions.

$$K_1 = \sqrt{2\pi} \cdot \lim_{r \to 0} \left[\left(\sigma_{\theta\theta} \right)_{\theta=0} \cdot r^{1-\lambda_1} \right] \tag{2}$$

The linear elastic, local stress component $\sigma_{\theta\theta}$ is calculated close to the notch tip ($r \to 0$) and along the notch bisector line (θ=0), as shown in the example of Fig. 12b. Finally, parameter λ_1 is correlated to the stress singularity degree (Williams, 1952) and is function of the opening angle 2α of the analysed V-notch (see Table 4).

Table 4: Values of parameters depending on the notch opening angle 2α.

2α (°)	λ_1 [a]	e_1 (ν=0.27) [b]	e_1 (ν=0.30) [c]
0	0.500	0.144	0.134
135	0.674	0.121	0.117

[a]: values from (Livieri and Lazzarin, 2005)
[b]: values valid for ADI 1050 calculated under plain strain conditions
[c]: values valid for S355J2 steel calculated under plain strain conditions

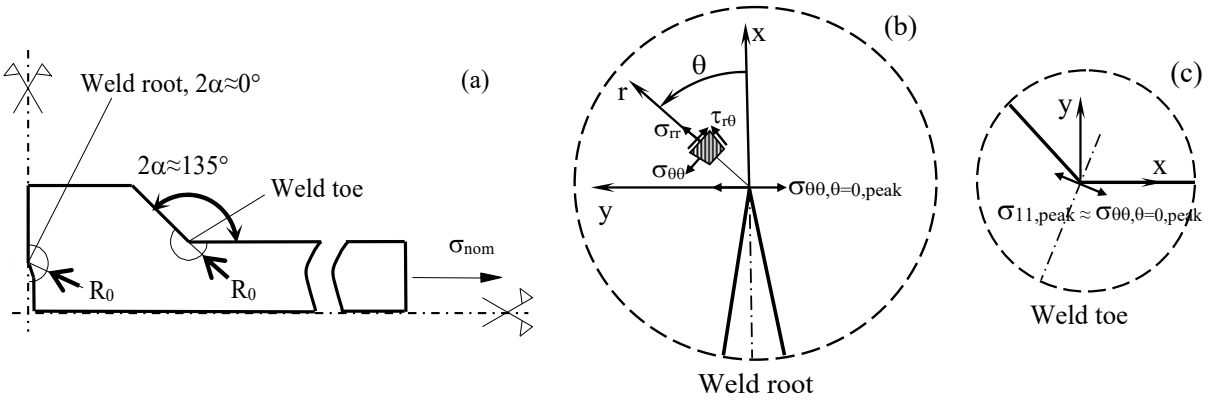

Figure 12: (a) Assumptions of the NSIF-based approach in fatigue design of welded joints referring to a partial-penetration butt joint under axial fatigue loading. The structural volume of radius R_0 centred either at the weld toe or at the weld root according to the averaged SED approach (b) Polar reference system (r,θ) centred at the weld root and local stress components. (b) and (c) Definition of peak stresses evaluated by means of a linear elastic finite element analysis at the weld toe and the weld root of a partial-penetration butt joint.

Lazzarin and collaborators (Lazzarin and Zambardi, 2001; Livieri and Lazzarin, 2005) assumed the strain energy density (SED) averaged over a structural volume surrounding the weld root or the weld toe as a fatigue strength criterion. They assumed a structural volume having circular shape with radius R_0 (see Fig. 12a) and provided the closed-form expression of the averaged SED parameter as a function of the relevant NSIFs. Dealing with a mode I fatigue loading condition (see Fig. 12), the SED averaged over the control volume can be expressed as follows (Lazzarin and Zambardi, 2001; Livieri and Lazzarin, 2005):

$$\Delta\overline{W} = \frac{e_1}{E}\left[\frac{\Delta K_1}{R_0^{1-\lambda_1}}\right]^2 \tag{3}$$

In Eq. (3), E represents the material modulus of elasticity; e_1 is a parameter dependent on the sharp notch geometry and on the material, through the opening angle 2α and the Poisson's ratio ν (see Table 4), respectively, while ΔK_1 is the range value of the NSIF relevant to mode I. Finally, R_0 represents the structural volume size.

A disadvantage in practical application of the NSIF-based approach is that very refined meshes are needed to calculate the NSIF by means of definition (2). The modelling procedure becomes particularly time-consuming for components that cannot be analysed by means of two-dimensional models. However, it has been shown that $\Delta\overline{W}$ can be estimated directly from FE analyses using coarse meshes inside the structural volume having radius R_0 (Lazzarin et al., 2010). Modelling the circular sector-shaped structural volume can be avoided and even more coarse FE meshes can be used thanks to the Peak Stress Method (PSM). The PSM is a rapid, numerical tool to rapidly estimate the NSIF K_1, taking advantage of the opening peak stress calculated from a linear elastic FE analysis with coarse mesh, as sketched in the example of Fig. 12b,c dealing with a partial-penetration butt joint. The estimated NSIF value can be obtained from the following expression (Meneghetti and Lazzarin, 2007):

$$K_1 \cong K^*_{FE} \cdot \sigma_{\theta\theta,\theta=0,peak} \cdot d^{1-\lambda_1} \tag{4}$$

In previous expression, $\sigma_{\theta\theta,\theta=0,peak}$ means that the opening stress acts in normal direction with respect to the notch bisector, as shown in Fig. 12b,c. Parameter d in Eq. (4) represents the average size of the finite elements which the FE analyst gives as input to the free mesh generation algorithm of the employed numerical software. Finally, parameter K^*_{FE} is dependent on the: (i) element type and formulation; (ii) FE mesh pattern and (iii) procedure employed by the numerical software to extrapolate stresses at nodes, as recently discussed in (Meneghetti et al., 2018). When adopting 4-node linear quadrilateral elements, as implemented in ANSYS® numerical code (PLANE 182 of Ansys element library with K-option 1 set to 3), K^*_{FE} resulted equal to 1.38 ± 3%, provided that a proper mesh pattern was adopted (see (Meneghetti and Lazzarin, 2007)) and the mesh density ratio a/d was greater than 3. When assessing the root side, a is the minimum value between the semi-crack length (crack is due to the lack of penetration) and the ligament length,

while *a* represents the plate thickness *t* when the toe side is taken into consideration.

It has been shown in Eq. (3) that the averaged SED can be expressed as a function of NSIF-term K_1, which the PSM allows to rapidly estimate through Eq. (4). Accordingly, the averaged SED can be rewritten as a function of the peak stress; moreover, by introducing the SED value for an equivalent uniaxial plane strain state, i.e. $W = \left(1-\nu^2\right)\sigma^2_{eq,peak} / 2E$, an equivalent peak stress can be defined by Eq. (5) (Meneghetti and Lazzarin, 2011):

$$\Delta\sigma_{eq,peak} = f_{w1} \cdot \Delta\sigma_{\theta\theta,\theta=0,peak} \tag{5}$$

Previous equation introduces parameter f_{w1}, which accounts for peak stress averaging inside the material-structural volume having size R_0, and it is defined as follows (Meneghetti and Lazzarin, 2011):

$$f_{w1} = K^*_{FE} \cdot \sqrt{\frac{2e_1}{1-\nu^2}} \cdot \left(\frac{d}{R_0}\right)^{1-\lambda_1} \tag{6}$$

Equations (4) and (6) show that both peak stress and coefficient f_{w1} are functions of the average element size *d* employed in the FE model to apply the PSM; however, the equivalent peak stress defined in Eq. (5), which includes the peak stress multiplied by f_{w1}, results to be independent of the average element size *d*.

A state-of-the-art review of the PSM has recently been published in (Meneghetti and Campagnolo, 2020), which the reader is referred to for additional details about the method.

6.2 Calibration of the structural volume size R_0 for ADI-to-steel arc-welded joints

The structural volume size R_0 to be adopted for the fatigue strength assessment of welded joints has been calibrated in (Lazzarin et al., 2003; Livieri and Lazzarin, 2005) by equalling the averaged SED in the following two situations:

- the high-cycle fatigue strength (typically at $N_A = 2 \cdot 10^6$ cycles) of welded joints exhibiting fatigue crack initiation either from the weld toe, where the opening angle is $2\alpha \approx 135°$, or from the weld root, $2\alpha \approx 0°$; i.e. the notched or cracked material;
- the high-cycle fatigue strength (again at $N_A = 2 \cdot 10^6$ cycles) of butt ground welded joints, i.e. the un-notched welded material.

The following equation was derived:

$$\Delta\bar{W}_{un-notched} = \Delta\bar{W}_{notched} \rightarrow \frac{\Delta\sigma_A^2}{2E} = \frac{e_1(2\alpha,\nu)}{E}\left(\frac{\Delta K_{1A}}{R_0^{1-\lambda_1}}\right)^2 \rightarrow R_0 = \left[\sqrt{2\cdot e_1(2\alpha,\nu)}\left(\frac{\Delta K_{1A}}{\Delta\sigma_A}\right)\right]^{\frac{1}{1-\lambda_1}} \tag{7}$$

As a result, R_0 was found to be 0.28 mm and 0.12 mm for homogeneous arc-welded joints made of structural steels or aluminium alloys (Lazzarin et al., 2003; Livieri and Lazzarin, 2005), respectively.

In principle, to apply the averaged SED approach to ADI-to-steel dissimilar arc-welded joints, it is first necessary to properly calibrate the structural volume size R_0. According to the damage analysis reported in previous sections, it has been observed that in the case of partial-penetration butt joints and T non-load-carrying fillet-welded joints the fatigue crack initiated and propagated through the material region made of structural steel. In all other cases, namely full-penetration butt joints and cruciform joints, the fatigue failure initiated at the weld toe or at the interface between the plate and the weld bead, always at the ADI side and more precisely in the ledeburite region. Therefore, in the case of partial-penetration butt joints and T nlc fillet-welded joints exhibiting fatigue crack initiation and propagation at the steel side, the structural volume size R_0 calibrated in previous papers for steel joints, i.e. $R_0 = 0.28$ mm, could be adopted to apply the averaged SED approach. On the other hand, in the case of fatigue crack initiation and propagation at the ADI side, the structural volume size R_0 should be re-calibrated by adopting the procedure proposed in (Livieri and Lazzarin, 2005).

Accordingly, first the high-cycle fatigue strength (at $N_A = 2 \cdot 10^6$ cycles) of welded joints exhibiting fatigue crack initiation at the weld toe at ADI side has to be derived in terms of range of the mode I NSIF, ΔK_1. To do this, the experimental results generated from welded joints fulfilling the following characteristics have been analysed:

- notch opening angle at the weld toe side $2\alpha = 135° \pm 5°$;
- nominal load ratio $R = 0.05$;

- fatigue failure at the weld toe on ADI side, where ledeburite is present.

Therefore, only a selection of joints belonging to series B1, C, E and F have been considered, since in some joints the notch opening angle 2α at the toe side was significantly higher than 135°, being equal to about 150°. After that, two-dimensional, plane strain FE models were defined in Ansys environment in order to convert the original experimental data from the nominal stress approach to the range of the mode I NSIF, ΔK_1, taking advantage of the PSM (Eq. (4)). The following assumptions have been made in the FE analyses (see also Fig. 13a):

- a sharp V-notch has been assumed at weld toe ($\rho = 0$) with $2\alpha = 135°$;
- a mono-material has been adopted, therefore modelling also steel regions as made by ADI 1050, with E=168000 MPa and ν=0.27.

Dealing with butt-welded joints, the actual geometry of the weld bead has been approximated in the FE models with a trapezoidal shape (see Table 5), according to (Meneghetti et al., 2015). A free mesh pattern of quadrilateral, 4-node PLANE 182 elements having a 'global element size' equal to *d* was generated. By doing so, a 2D FE mesh of the type shown in the examples of Fig. 5 was obtained. The mesh size *d* was chosen in order to comply with the conditions of applicability of the PSM, i.e. $a/d = 3 \rightarrow d = a/3$. After having calculated the opening peak stress $\sigma_{\theta\theta,\theta=0,peak}$ at the weld toe side, the ΔK_1 has been calculated from Eq. (4). The experimental results expressed in terms of number of cycles to failure as a function of ΔK_1 have been reported in Fig. 13b, where it can be observed that at $N_A = 2 \cdot 10^6$ cycles and with reference to a survival probability of 50%, ΔK_{1A} equals 475 MPa·mm^{326}.

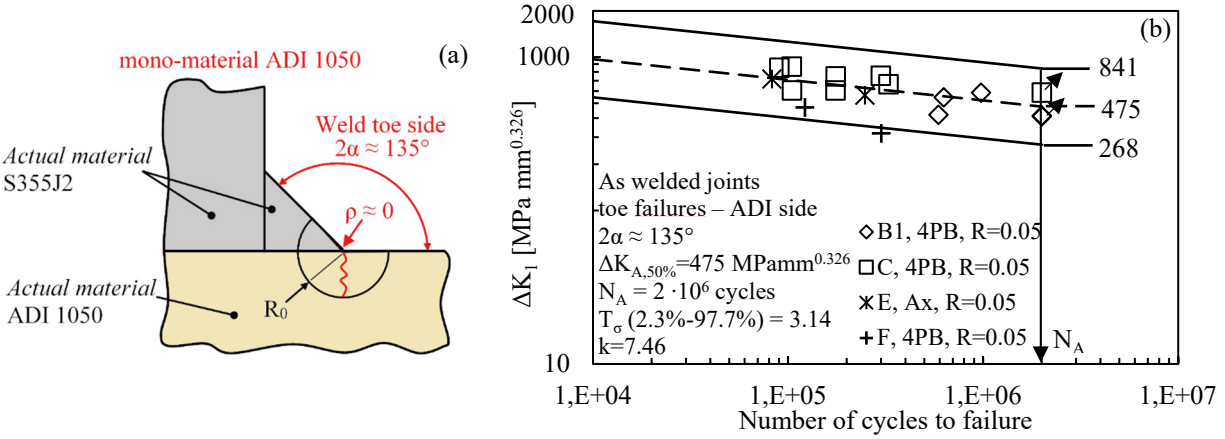

Figure 13: (a) Assumptions made in the FE analyses according to PSM. (b) Synthesis of a selection of experimental results reported in Figs. 10b,e,g,h in terms of number of cycles to failure as a function of the range of the mode I NSIF ΔK_1.

The high-cycle fatigue strength (again at $N_A = 2 \cdot 10^6$ cycles) of butt ground welded joints under axial loading being equal to $\Delta\sigma_A = 287$ MPa according to Fig. 10c, the control radius R_0 for ADI-to-steel joints exhibiting fatigue failure at weld toe at ADI side has been evaluated as follows:

$$R_0 = \left[\sqrt{2}\cdot e_1(135°, 0.27)\left(\frac{\Delta K_{1A}}{\Delta\sigma_A}\right)^{\frac{1}{1-\lambda_1}}\right] = \left[\sqrt{2}\cdot 0.121\left(\frac{475\text{MPa}\cdot\text{mm}^{0.326}}{287\text{MPa}}\right)^{\frac{1}{0.326}}\right] = 0.53\text{mm} \quad (8)$$

It is worth noting that $R_0 = 0.53$ mm for ADI-to-steel joints is significantly greater than $R_0 = 0.28$ mm, which was calibrated in previous papers for homogeneous steel joints (Lazzarin et al., 2003; Livieri and Lazzarin, 2005).

6.3 PSM-based synthesis of experimental fatigue results relevant to ADI-to-steel arc-welded joints

Two-dimensional, plane strain FE models were defined in the present paper in order to convert the original experimental data from the nominal stress approach (Fig. 11) to the equivalent peak stress parameter. The assumptions sketched in Fig. 13a have been adopted in all FE analyses. Only one quarter of each welded joint was modelled, taking advantage of the double symmetry, as shown in Table 5, which reports only two examples for sake of brevity.

Again, a free mesh pattern of quadrilateral, 4-node PLANE 182 elements having a 'global element size' equal to *d* was generated (see Table 5), the mesh size *d* being chosen in order to comply with the conditions of applicability of

the PSM, i.e. $a/d = 3 \rightarrow d = a/3$. After having calculated the opening peak stress $\sigma_{\theta\theta,\theta=0,peak}$ at the weld toe side, the equivalent peak stress has been calculated from Eq. (5), with f_{w1} relevant to $R_0 = 0.53$ mm.

Table 5: Examples of FE analyses for fatigue strength assessment according to the PSM.

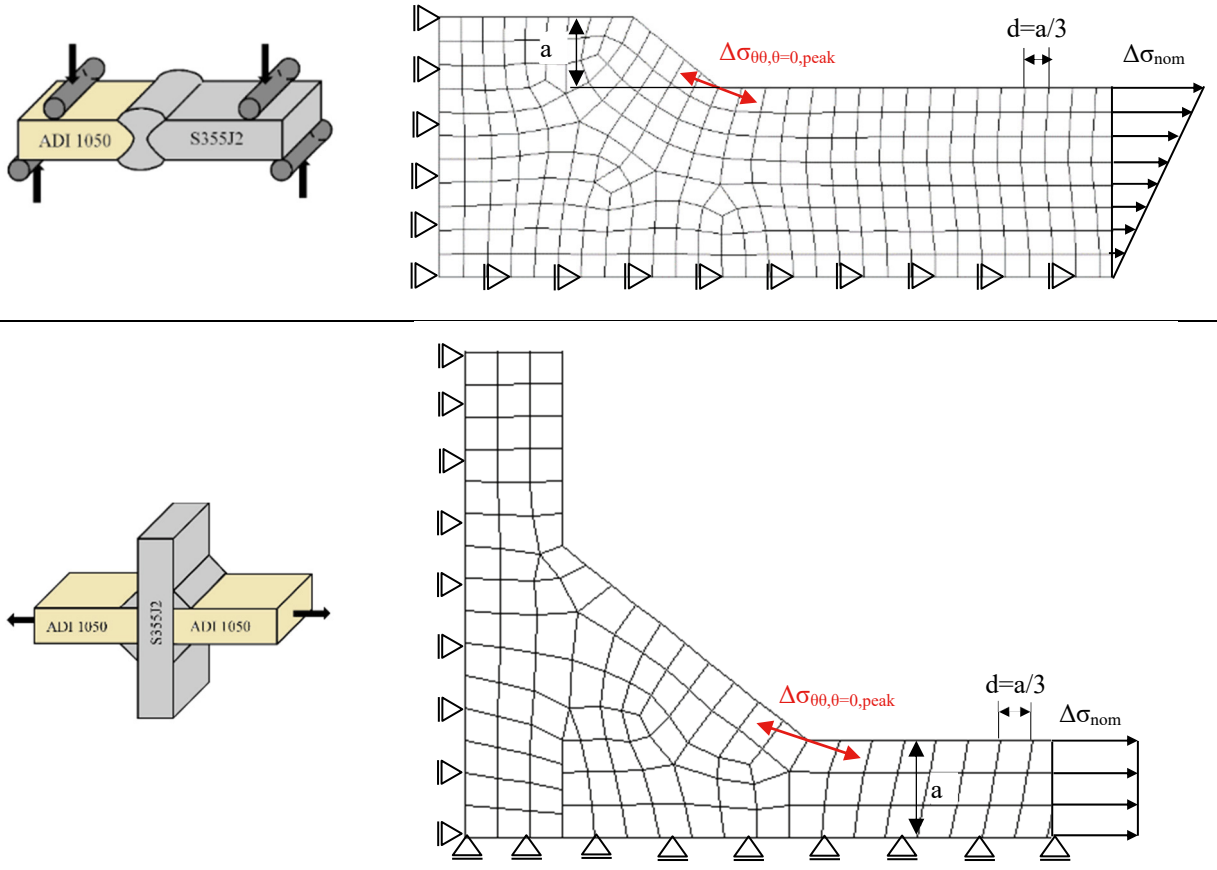

The experimental results expressed in terms of number of cycles to failure as a function of the equivalent peak stress have been reported in Fig. 14, which includes also a 2.3-97.7% scatter-band calibrated on all considered experimental results and, for comparison purposes, also the PSM-based fatigue curve referred to 97.7% survival probability, as calibrated in (Meneghetti and Lazzarin, 2011) for homogeneous steel welded joints.

The resulting fatigue design curve for ADI-to-steel joints exhibiting fatigue failure at weld toe at ADI side is characterised by a fatigue class of $\Delta\sigma_{eq,peak,A,97.7\%} = 160$ MPa, an inverse slope $k = 8.9$ and a scatter index $T_\sigma = 2.71$, which is significantly reduced with respect to the scatter index obtained in Fig. 11 by synthesizing the same experimental results but in terms of nominal stress range.

It is worth noting that the fatigue design curve for ADI-to-steel joints provide almost the same fatigue strength of the curve for homogeneous steel joints at $N_A = 2 \cdot 10^6$ cycles (160 MPa versus 156 MPa), while the fatigue strength of ADI-to-steel joints is significantly lower than that of homogeneous steel joints at medium cycle fatigue regime. This is due to the different inverse slope k, which equals 8.9 for ADI-to-steel joints, while it is 3 for homogeneous steel joints.

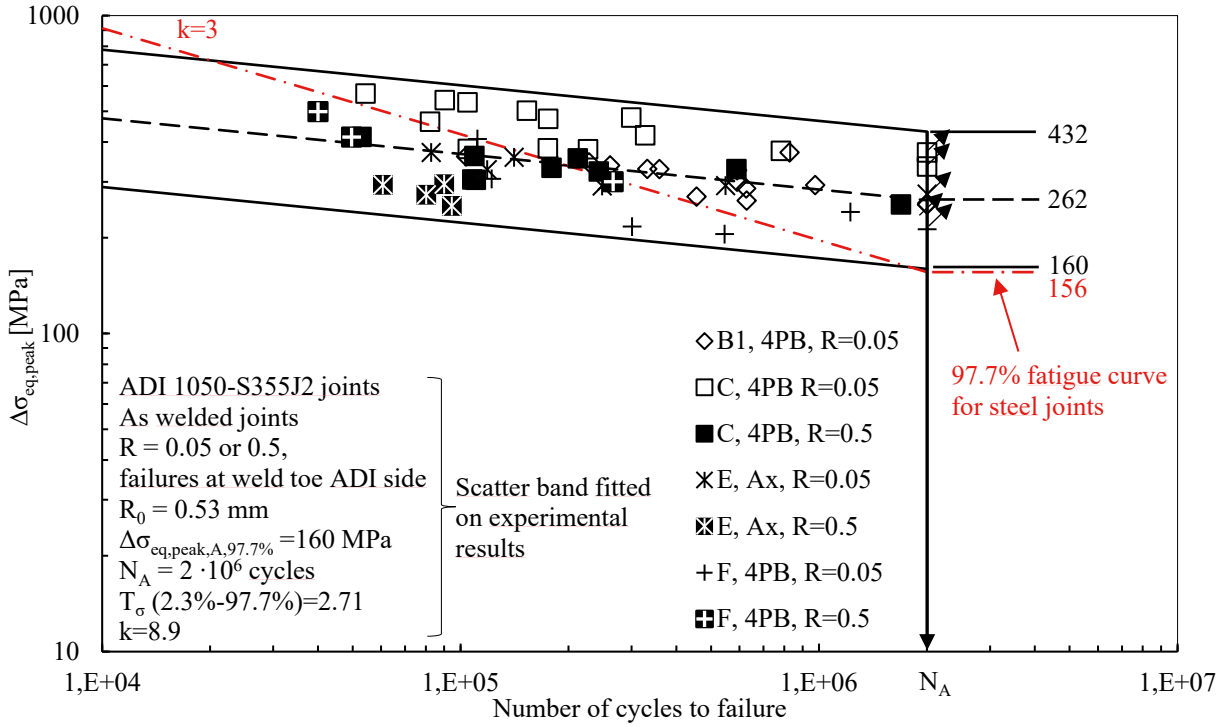

Figure 14: Synthesis of experimental results reported in Figs. 10b,e,g,h in terms of number of cycles to failure as a function of the range of the equivalent peak stress.

7. Conclusions

In the present paper, the fatigue behaviour of austempered ductile iron (EN-JS-1050)-to-steel (S355J2) dissimilar arc-welded joints has been experimentally investigated. The strength categories of some typical welded details were derived and compared with the categories provided by standards and recommendations for homogeneous steel welded joints. All joints were tested in the as-welded conditions. It can be concluded that:

- fatigue crack initiated at weld toe at ADI side, i.e. at the ledeburite region, where hardness is about 700HV as compared to 350-400HV of the ADI base material. The only exceptions are partial-penetration butt joints and T nlc fillet-welded joints where crack initiated and propagated within the steel material region.
- the endurable stresses, referred to N_A= 2 million cycles, 97.7% survival probability and 95% of confidence level, of ADI-to-steel dissimilar joints are higher than those suggested by International Standards for the corresponding homogeneous steel welded joints.
- the local fatigue approach based on the combination of the Peak Stress Method with the averaged Strain Energy Density criterion has been calibrated to be applied to ADI-to-steel dissimilar joints exhibiting crack initiation at the weld toe at ADI side. The structural volume size results in R_0 = 0.53 mm. The fatigue design curve expressed in terms of number of cycles to failure as a function of the equivalent peak stress has been calibrated on experimental results and gives: $\Delta\sigma_{eq,peak,A,97.7\%}$ = 160 MPa, k = 8.9, T_σ = 2.71.

References

Al Zamzami, I., Davison, B., Susmel, L., 2019. Nominal and local stress quantities to design aluminium-to-steel thin welded joints against fatigue. Int. J. Fatigue 123, 279–295. doi:10.1016/J.IJFATIGUE.2019.02.018

Atzori, B., Meneghetti, G., 2001. Fatigue strength of fillet welded structural steels: finite elements, strain gauges and reality. Int. J. Fatigue 23, 713–721. doi:10.1016/S0142-1123(01)00028-7

Carpinteri, A., Spagnoli, A., Vantadori, S., 2009. Multiaxial fatigue life estimation in welded joints using the critical plane

approach. Int. J. Fatigue 31, 188–196. doi:10.1016/j.ijfatigue.2008.03.024
Eurocode 3: Design of steel structures – part 1–9: Fatigue, 2005. . CEN.
Eurocode 9: Design of aluminium structures - Part 1-3: Structures susceptible to fatigue, 2011. . CEN.
Figner, G., Vallant, R., Weinberger, T., Enzinger, N., Schröttner, H., Paśič, H., 2009. Friction Stir Spot Welds between Aluminium and Steel Automotive Sheets: Influence of Welding Parameters on Mechanical Properties and Microstructure. Weld. World 53, R13–R23. doi:10.1007/BF03266697
Gross, B., Mendelson, A., 1972. Plane elastostatic analysis of V-notched plates. Int. J. Fract. Mech. 8, 267–276. doi:10.1007/BF00186126
Hobbacher, A.F., 2016. Recommendations for Fatigue Design of Welded Joints and Components, IIW Collection. IIW Collection. Springer International Publishing. doi:10.1007/978-3-319-23757-2
Infante, V., Braga, D.F.O., Duarte, F., Moreira, P.M.G., de Freitas, M., de Castro, P.M.S.T., 2016. Study of the fatigue behaviour of dissimilar aluminium joints produced by friction stir welding. Int. J. Fatigue 82, 310–316. doi:10.1016/j.ijfatigue.2015.06.020
Kumar, S., Singh, P.K., Karn, K.N., Bhasin, V., 2017. Experimental investigation of local tensile and fracture resistance behaviour of dissimilar metal weld joint: SA508 Gr.3 Cl.1 and SA312 Type 304LN. Fatigue Fract. Eng. Mater. Struct. 40, 190–206. doi:10.1111/ffe.12484
Lazzarin, P., Berto, F., Zappalorto, M., 2010. Rapid calculations of notch stress intensity factors based on averaged strain energy density from coarse meshes: Theoretical bases and applications. Int. J. Fatigue 32, 1559–1567. doi:10.1016/j.ijfatigue.2010.02.017
Lazzarin, P., Lassen, T., Livieri, P., 2003. A notch stress intensity approach applied to fatigue life predictions of welded joints with different local toe geometry. Fatigue Fract. Eng. Mater. Struct. 26, 49–58. doi:10.1046/j.1460-2695.2003.00586.x
Lazzarin, P., Livieri, P., 2001. Notch stress intensity factors and fatigue strength of aluminium and steel welded joints. Int. J. Fatigue 23, 225–232. doi:10.1016/S0142-1123(00)00086-4
Lazzarin, P., Tovo, R., 1998. A notch intensity factor approach to the stress analysis of welds. Fatigue Fract. Eng. Mater. Struct. 21, 1089–1103. doi:10.1046/j.1460-2695.1998.00097.x
Lazzarin, P., Zambardi, R., 2001. A finite-volume-energy based approach to predict the static and fatigue behavior of components with sharp V-shaped notches. Int. J. Fract. 112, 275–298. doi:10.1023/A:1013595930617
Livieri, P., Lazzarin, P., 2005. Fatigue strength of steel and aluminium welded joints based on generalised stress intensity factors and local strain energy values. Int. J. Fract. 133, 247–276. doi:10.1007/s10704-005-4043-3
Martinsen, K., Hu, S.J., Carlson, B.E., 2015. Joining of dissimilar materials. CIRP Ann. 64, 679–699. doi:10.1016/j.cirp.2015.05.006
Meneghetti, G., Campagnolo, A., 2020. State-of-the-art review of peak stress method for fatigue strength assessment of welded joints. Int. J. Fatigue 139, 105705. doi:10.1016/j.ijfatigue.2020.105705
Meneghetti, G., Campagnolo, A., Avalle, M., Castagnetti, D., Colussi, M., Corigliano, P., De Agostinis, M., Dragoni, E., Fontanari, V., Frendo, F., Goglio, L., Marannano, G., Marulo, G., Moroni, F., Pantano, A., Rebora, A., Scattina, A., Spaggiari, A., Zuccarello, B., 2018. Rapid evaluation of notch stress intensity factors using the peak stress method: Comparison of commercial finite element codes for a range of mesh patterns. Fatigue Fract. Eng. Mater. Struct. 41. doi:10.1111/ffe.12751
Meneghetti, G., Campagnolo, A., Berto, D., Pullin, E., Masaggia, S., 2019a. Fatigue properties of austempered ductile iron-to-steel dissimilar arc-welded joints, in: IIW Annual Assembly. IIW Doc. XIII-2786-19. Bratislava (Slovakia).
Meneghetti, G., Campagnolo, A., Berto, D., Pullin, E., Masaggia, S., 2019b. Fatigue properties of austempered ductile iron-to-steel dissimilar arc-welded joints. Procedia Struct. Integr. 24, 190–203. doi:10.1016/j.prostr.2020.02.016
Meneghetti, G., Campagnolo, A., Berto, F., 2015. Fatigue strength assessment of partial and full-penetration steel and aluminium butt-welded joints according to the peak stress method. Fatigue Fract. Eng. Mater. Struct. 38, 1419–1431. doi:10.1111/ffe.12342
Meneghetti, G., Lazzarin, P., 2011. The Peak Stress Method for Fatigue Strength Assessment of welded joints with weld toe or weld root failures. Weld. World 55, 22–29. doi:10.1007/BF03321304
Meneghetti, G., Lazzarin, P., 2007. Significance of the elastic peak stress evaluated by FE analyses at the point of singularity of sharp V-notched components. Fatigue Fract. Eng. Mater. Struct. 30, 95–106. doi:10.1111/j.1460-2695.2006.01084.x
Mohammadzadeh Polami, S., Häfele, P., Rethmeier, M., Schmid, A., 2015. Study on fatigue behavior of dissimilar materials and different methods of friction-welded joints for drive pinion in trucks. Weld. World 59, 917–926. doi:10.1007/s40194-015-0258-8
Okamura, H., Aota, K., 2004. Joining of dissimilar materials with friction stir welding. Weld. Int. 18, 852–860. doi:10.1533/wint.2004.3344
Radaj, D., Sonsino, C.M., Fricke, W., 2006. Fatigue Assessment of Welded Joints by Local Approaches, 2nd ed. Woodhead Publishing, Cambridge.
Roberts, D.I., Ryder, R.H., Viswanathan, R., 1985. Performance of Dissimilar Welds in Service. J. Press. Vessel Technol. 107, 247. doi:10.1115/1.3264443
Sonsino, C., 1995. Multiaxial fatigue of welded joints under in-phase and out-of-phase local strains and stresses. Int. J. Fatigue 17, 55–70. doi:10.1016/0142-1123(95)93051-3

Susmel, L., 2009. Multiaxial notch fatigue. Woodhead Publishing, Cambridge, UK.
Susmel, L., 2008. Modified Wöhler curve method, theory of critical distances and Eurocode 3: A novel engineering procedure to predict the lifetime of steel welded joints subjected to both uniaxial and multiaxial fatigue loading. Int. J. Fatigue 30, 888–907. doi:10.1016/j.ijfatigue.2007.06.005
Taban, E., Gould, J.E., Lippold, J.C., 2010. Dissimilar friction welding of 6061-T6 aluminum and AISI 1018 steel: Properties and microstructural characterization. Mater. Des. 31, 2305–2311. doi:10.1016/J.MATDES.2009.12.010
Taylor, D., Barrett, N., Lucano, G., 2002. Some new methods for predicting fatigue in welded joints. Int. J. Fatigue. doi:10.1016/S0142-1123(01)00174-8
Uzun, H., Dalle Donne, C., Argagnotto, A., Ghidini, T., Gambaro, C., 2005. Friction stir welding of dissimilar Al 6013-T4 To X5CrNi18-10 stainless steel. Mater. Des. 26, 41–46. doi:10.1016/j.matdes.2004.04.002
Williams, M.L., 1952. Stress singularities resulting from various boundary conditions in angular corners of plates in tension. J Appl Mech 19, 526–528.
Zhang, W.-C., Zhu, M.-L., Wang, K., Xuan, F.-Z., 2018. Failure mechanisms and design of dissimilar welds of 9%Cr and CrMoV steels up to very high cycle fatigue regime. Int. J. Fatigue 113, 367–376. doi:10.1016/j.ijfatigue.2018.04.032